Available online at www.sciencedirect.com
ScienceDirect
Journal of Power Sources 162 (2006) 1437–1443
JOURNAL OF POWER SOURCES
www.elsevier.com/locate/jpowsour

# Electrochemical characterization on $MnFe_2O_4$/carbon black composite aqueous supercapacitors

Shin-Liang Kuo, Nae-Lih Wu *

*Department of Chemical Engineering, National Taiwan University, Taipei 106, Taiwan, ROC*

Received 17 April 2006; received in revised form 24 July 2006; accepted 31 July 2006
Available online 12 September 2006

**Abstract**

$MnFe_2O_4$–carbon black (CB) composite powders synthesized by a co-precipitation method have been characterized and optimized for their electrochemical properties for supercapacitor applications. The composite shows pseudocapacitance in electrolyte solutions of alkali and alkaline chlorides, sulfates and sulfites. For the chlorides and sulfates electrolytes, the pseudocapacitance has been identified, by *in situ* X-ray absorption near-edge spectroscopy study, to involve charge-transfer at both the Mn and Fe sites of the ferrite. In 1 M $NaCl_{(aq)}$, the composite electrode exhibits an operating potential window of 1.0 V with a maximum leakage current of 0.3 mA $F^{-1}$, and it exhibits far superior cycling stability to amorphous $MnO_2$ electrode. Both the specific capacitance and self-discharge behavior of the composite electrode depend strongly on the composite composition. The optimum capacitance occurs at ferrite:CB weight ratio of 7:3, which gives reduced self-discharge rate as compared with CB. The composite electrode also demonstrates capability of high-power delivery.


*Keywords:* Supercapacitor; Manganese ferrite; Pseudocapacitance

## 1. Introduction

Electrochemical capacitor, also known as supercapacitor, is a promising energy storage device for meeting the high-power electric market [1–3]. In addition to the well-established carbon-based electric double-layer capacitors, there has been continuing research in exploring new materials exhibiting pseudocapacitance behaviors for the supercapacitor applications. Pseudocapacitance results from either superficial or multi-electron-transfer faradaic reactions with fast charge/discharge properties. Electrochemically, a pseudocapacitor behaves like a capacitor, rather than a galvanic cell.

The first known pseudocapacitive oxide is hydrated amorphous ruthenium oxide, $RuO_2$ [4]. Although it has demonstrated specific capacitances up to 700 F $g^{-1}$ and high-power density in strong acidic aqueous electrolyte [5,6], its extraordinarily high cost has limited its large-scale applications. Hydrated amorphous manganese oxide, a-$MnO_2$, was subsequently discovered in 1999 [7,8] to exhibit pseudocapacitance in neutral NaCl and KCl solutions. Because of its low cost and environmental benignity, the manganese oxide has ever since drawn much attention [7–11]. However, its poor cycling stability is the main obstacle to overcome. $Fe_3O_4$ is another newly discovered inexpensive pseudocapacitive material, exhibiting pseudocapacitance in alkali sulfites electrolytes [12–14]. Its pseudocapacitance has been shown to arise from redox reactions of adsorbed sulfite anions involving at maximum six-electron transfer [15]. It is the only material of which the pseudocapacitance is associated with anion, rather than cations as in the cases of $RuO_2$ and a-$MnO_2$. However, the electron-transfer kinetics involved may not be fast enough for high-power applications.

We have recently reported [16] that some crystalline ferrite oxides, particularly $MnFe_2O_4$ and $CoFe_2O_4$, also exhibited pseudocapacitance in NaCl solution, bearing certain resemblance to a-$MnO_2$. In this work, composite powders consisting of nanocrystalline $MnFe_2O_4$ and porous carbon black (CB) have been prepared, and they were characterized and optimized for their electrochemical properties, including specific capacitance, operating potential window, leakage current, self-discharge, and cycling stability. Comparison was also made between the current composite powders and a-$MnO_2$ for some of these properties. In brief, the $MnFe_2O_4$–CB composite exhibits superior cycling

* Corresponding author. Tel.: +886 2 23627158; fax: +886 2 23623040.
*E-mail address:* nlw001@ntu.edu.tw (N.-L. Wu).

0378-7753/$ – see front matter © 2006 Elsevier B.V. All rights reserved.
doi:10.1016/j.jpowsour.2006.07.056

stability to a-$MnO_2$, and it has demonstrated high-power delivering capability.

## 2. Experimental

$MnFe_2O_3$/carbon black (CB; VULCAN® XC72, Cabot Corp., U.S.A.) composite powders have been prepared by a co-precipitation method in alkaline aqueous solutions as follows. $MnSO_4$ was dissolved along with $FeCl_3$ with a stoichiometric ratio of 2:1 in 1 M HCl aqueous solution with bubbling $N_2$. The solution is then added into another solution that contains 1.5 M NaOH and suspended CB powder under vigorous stirring. Black precipitate was formed immediately upon mixing. It was found that the CB particles sedimented simultaneously with the oxide precipitate, suggesting that the oxide component was homogeneously combined with the CB particles during the synthesis process. The supernatant liquid was then decanted and fresh de-ionized water was added. The consecutive solution-decanting and water-replenishing processes were carried out to remove residual anions. The powder was prepared by drying at 50 °C. A subsequent calcination process was carried out at different temperatures for 2 h in $N_2$ atmosphere.

Amorphous $MnO_2$ (a-$MnO_2$) powder has also been prepared for comparison study. The powder was precipitated by mixing 0.15 M $KMnO_4$ and 0.15 M $MnSO_4$ aqueous solutions with an Mn(VII)/Mn(II) molar ratio of 2:3 at 25 °C. After thoroughly washed with de-ionized water, the particles were finally heated at 200 °C for 1 h in air.

Synchrotron analyses were conducted with the beam-line 01-C2 (for X-ray diffraction; XRD) and 17-C1 (for X-ray absorption near-edge spectroscopy; XANES) facilities of the National Synchrotron Radiation Research Center (NSRRC) in Taiwan. XRD was performed with a beam wavelength $\lambda = 0.061993$ nm. For *in situ* XANES experiment, cyclic voltammetry (CV) ran at a scan-rate of 0.2 mV $s^{-1}$, and the potential was stopped at each of the selected values for 10 min for data collection. The test cell was made of acrylics, and the two sides of the cell were perforated and then sealed with Kapton foils in order to allow the probing beam to pass through the cell.

Transmission micrographs were carried out on a transmission electron microscopy (TEM; H7100). BET surface areas and pore size distributions were determined by nitrogen adsorption (ASAP 2010, Micrometrics).

Supercapacitor electrodes were made of the ferrite/CB composite powders, PVdF in 10 wt.% and Ti-foil current collector, and they were finally dried at 120 °C for 6 h in vacuum. For the a-$MnO_2$ electrode, the oxide to CB ratio was fixed at 8:2 by weight, and it was dried in air. Electrochemical characterizations were carried out with a three-electrode cell with Pt mesh and Ag/AgCl/saturated KCl (EG&G, 197 mV versus NHE at 25 °C) as the counter and reference electrode, respectively. Symmetric cell configuration having one of the two identical composite electrodes as the reference was also adopted for some of the experiments. The electrolyte solution was 1 M salt aqueous solution. The *CV* curves were recorded by an electrochemical analyzer (Eco Chemie PGSTAT30). The average specific capacitance of the electrodes was calculated by

$$C_{\text{avg}} = \frac{\Delta Q}{w\Delta V} = \frac{\left(\int I\,\mathrm{d}V\right)/s}{\Delta V/w} \quad (1)$$

where $\Delta Q$ is the total amount of charge accumulated over a potential window $\Delta V$; $w$ the mass of active material in an electrode; $I$ the current; $s$ is the potential scan-rate.

## 3. Results

### 3.1. Microstructural characterizations

Microstructural and electrochemical characterizations have been carried out mainly on the powder with the ferrite to CB weight ratio of 1:1. Optimization of CB content has also been carried out based on the overall specific capacitance. As previously reported [16], the precipitate powder starts to exhibit capacitive behavior only when calcination was carried out at temperatures above 300 °C. Fig. 1 shows the synchrotron XRD patterns of the powders calcined between 300 and 400 °C. All the important reflections of the spinel $MnFe_2O_3$ phase began to appear at 300 °C, and the peaks became increasingly sharpened with increasing calcination temperature. The average crystallite sizes have been determined by using the Scherrer equation based on the full width at half maximum intensity of the (3 1 1) peak of the ferrite phase, and they are listed in Table 1. The ferrite crystallite size increases from 2.5 to ~23 nm as the calcination temperature increases from 300 to 500 °C.

TEM micrograph of the powder calcined at 350 °C is shown in Fig. 2. Two different types of particles can be distinguished. The CB particles show granular appearance with sizes ranging from 50 to 70 nm, while the ferrite particles, which appear darker and randomly dispersed onto CB surface, exhibit sizes ranging from a few to ~10 nm. The sizes of the ferrite particles are close to the crystallite size determined by XRD (Table 1), indicating that every particle is basically a single crystal.

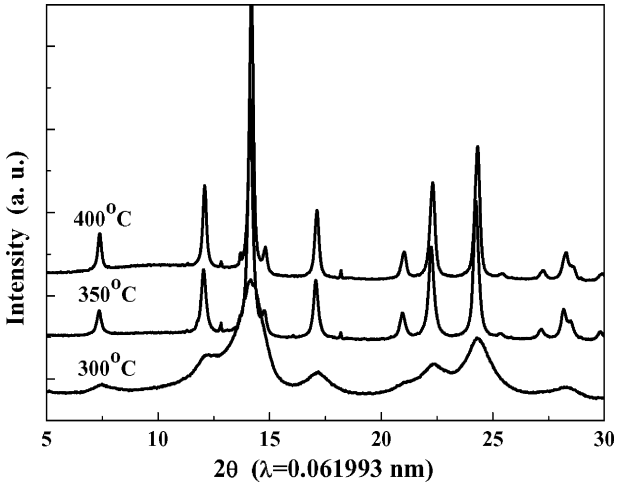


Fig. 1. X-ray diffraction patterns of the co-precipitated $MFe_2O_4$/carbon black powders calcined at different temperatures.

Table 1
The microstructural and electrochemical data of $MnFe_2O_4$/carbon black (weight ratio = 1:1) composite powders in 1 M NaCl solution

| Sample no. | Calcination temperature (°C) | Crystallite size (nm) | Specific capacitance (F (g composite)$^{-1}$) |
|---|---|---|---|
| 1 | 300 | 2.5 | 50.6 |
| 2 | 350 | 13.2 | 56.2 |
| 3 | 400 | 17.6 | 41.6 |
| 4 | 500 | 23.2 | 14.8 |

Fig. 3 shows the BJH pore size distributions and BET surface areas for both CB and the 350 °C-calcined composite powders. The CB powder has a porous structure containing predominantly mesopores with a total pore volume of 0.48 $cm^3\ g^{-1}$. The specific surface area is about 220 $m^2\ g^{-1}$, of which one-third is associated with micropores. The presence of the ferrite particles appears not dramatically to alter the pore distribution and pore volume originally presented in the CB substrate. This ensures the presence of sufficient voids in the electrode to serve as electrolyte reservoirs, which will be important for high rate capability. On the other hand, the surface area did exhibit a quite significant decline, from 220 $m^2\ g^{-1}$ for pure CB to 160 $m^2\ g^{-1}$ for the 350 °C-composite. As shown in Fig. 3b, the loss is mainly within the pore diameter range below 3 nm. A significant portion of the micropores of the CB substrate was likely filled up with the resulting ferrite particles, causing the surface area reduction. The surface area further decreases to 92 $m^2\ g^{-1}$ when calcination temperature was raised to 500 °C. This change is believed to result from coarsening and agglomeration of $MnFe_2O_4$ crystallites. As shown in Table 1, the capacitances of the composite powder first increase and then decrease with calcination temperature with the maximum taking place at 350 °C. The initial capacitance increase with temperature can be attributed to improved crystallinity of the ferrite phase [16], while the reduction at higher temperatures is due to the loss in surface area for both CB and ferrite.

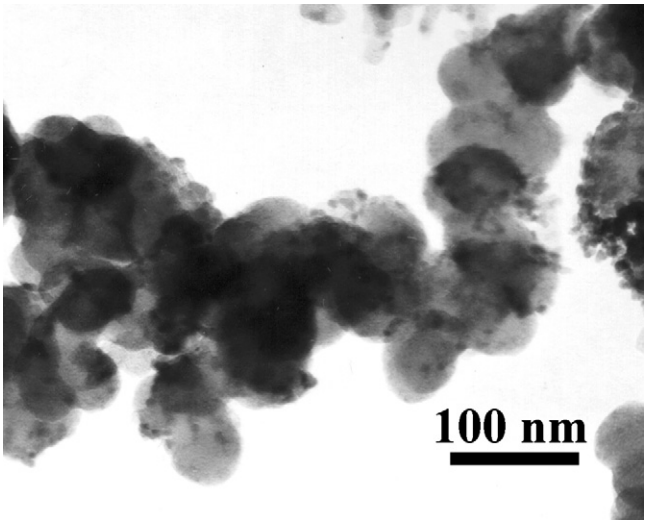


Fig. 2. TEM micrograph of $MnFe_2O_4$/carbon black composite powder with the weight ratio of 1:1.

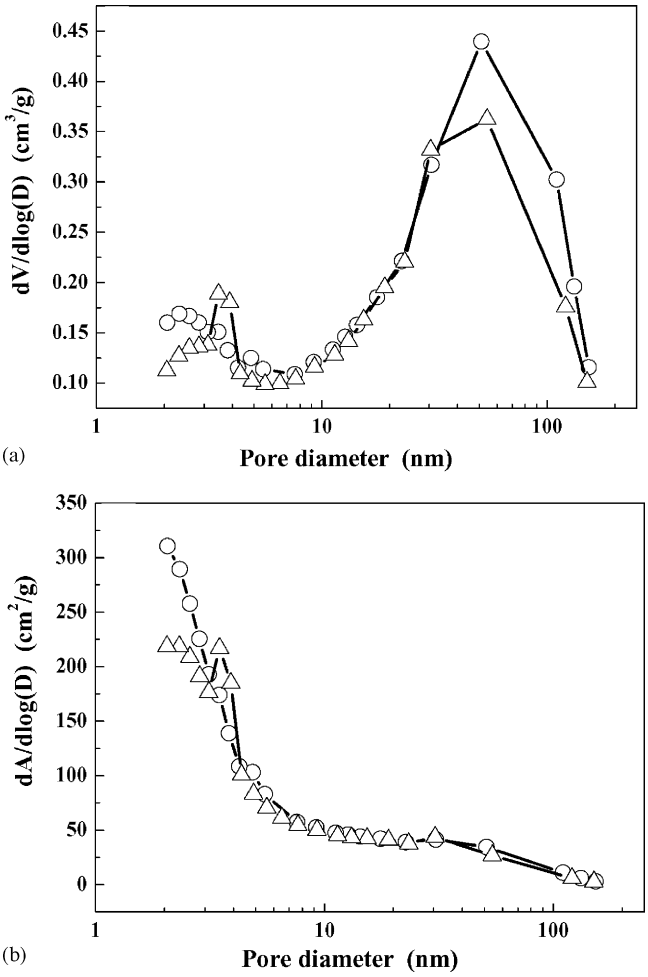


Fig. 3. (a) The BJH pore volume ($V$) distributions and (b) the surface area ($A$) distributions of (◯) CB and (△) $MnFe_2O_4$/CB composite powder calcined at 350 °C. $D$ represents pore diameter.

### 3.2. Electrochemical and spectroscopic analyses

Fig. 4 compares the voltammograms of single composite (ferrite:CB = 1:1) electrode performed in 1 M aqueous solutions of MCl, where M = Li, Na, K, and Cs, and $CaCl_2$ electrolytes at the scan-rate of 20 mV $s^{-1}$. The curves show similar line profiles, exhibiting fairly rectangular shape with a couple of broad redox peaks within intermediate potential range. The electrode exhibits the largest capacitance (56 F $g^{-1}$) in $NaCl_{(aq)}$ and the smallest value, 43.5 F $g^{-1}$-$MnFe_2O_4$, in $CsCl_{(aq)}$.

By switching the anion of the electrolyte from $Cl^-$ to $SO_4{}^{2-}$, there was observed a significant (∼30%) reduction in capacitance, but the line profile remains essentially the same (Fig. 5), meaning that the fundamental charge-transfer mechanism has not been changed. In contrast, when the sulfite salt, $Na_2SO_3$, is used, the potential window for pseudocapacitance shifts markedly to lower potentials, between −0.8 and 0.1 V, and the line profile becomes completely different. In fact, the line profile bears great resemblance to what has been seen for $Fe_3O_4$ in the same electrolyte [15], and it has been attributed to the redox reactions of the sulfite anions. This reaction mechanism is apparently not applicable to the solutions of either the chlo-

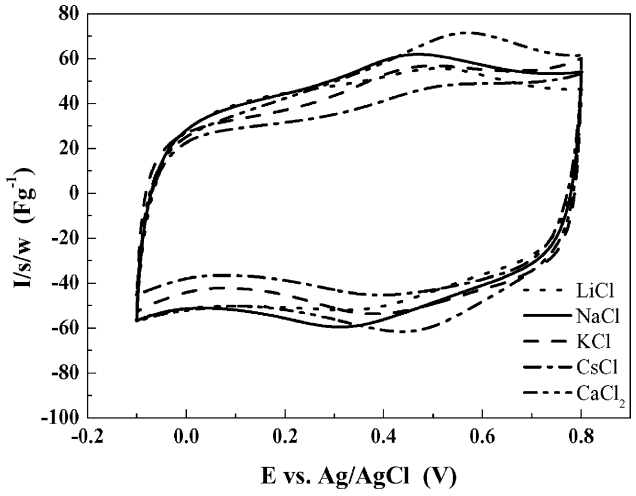


Fig. 4. Voltammograms of $MnFe_2O_4$/CB composite electrode in different alkali and alkaline salt electrolytes. Scan-rate is 20 mV $s^{-1}$.

ride or sulfate salts. This study will focus mainly on the chloride electrolyte solutions.

Fig. 6a and b shows respectively the Mn and Fe K-edge XANES spectra of the composite electrode acquainted *in situ* during a cathodic scan from 0.8 to −0.1 V with respect to Ag/AgCl. The main edge energy is known to increase with increasing valence of the detected metal ion [17]. As shown, the K-edge energies for both Mn and Fe shift to lower energies, suggesting decrease in valence, during the cathodic sweep. The edge energies were found to shift back to higher energies during the subsequent oxidative sweep (not shown). These results give direct evidence to charge-transfer at both the Mn and Fe sites, and the origin of the capacitance is indeed pseudocapacitance in nature.

The tests for capability of high-power delivery and cycle stability were carried out by adopting the symmetric cell configuration. The voltammograms of the symmetric cell in different chloride salts solution are shown in Fig. 7. The profiles are consistent with what can be deduced from the data of the three-electrode

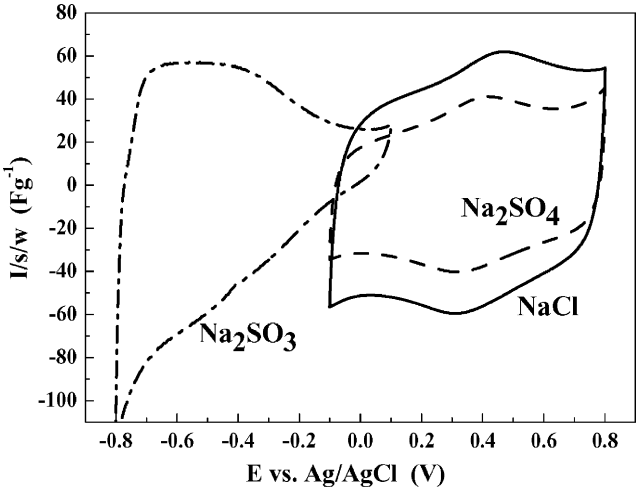


Fig. 5. Voltammograms of $MnFe_2O_4$/CB composite electrode in different anion-substituted electrolytes. Scan-rate is 20 mV $s^{-1}$.

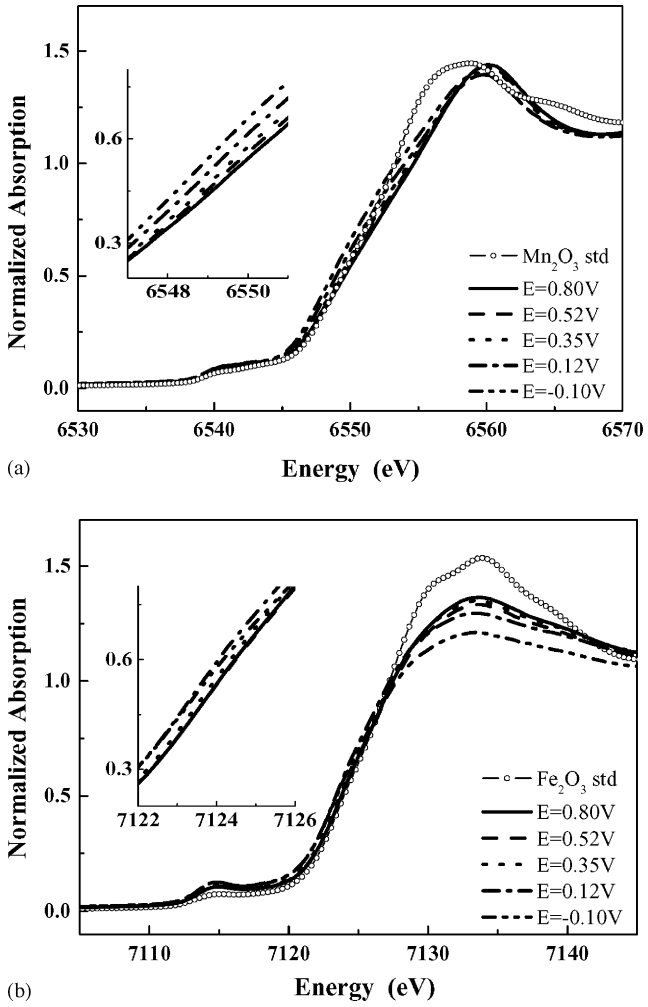


Fig. 6. (a) The Mn K-edge and (b) Fe K-edge XANES spectra taken *in situ* along the course of reduction in 1 M $KCl_{(aq)}$. The insets enlarge the center portion of the main absorption edges.

configuration (Fig. 4). The data for the rate dependence of capacitance were collected in Fig. 8. In general, the rate dependence is insensitive to the type of cation in the electrolyte, and it decreases by ∼15% as the scan-rate increases from 20 to 200 mV $s^{-1}$, except for the case of KCl showing a less reduction, ∼9%.

Fig. 9 depicts the voltammograms of a symmetric cell collected at temperature ranging from 0 to 20 °C. All the current profiles still exhibited the characteristics of a capacitor but slight reduction in current with decreasing operating temperature was noticed. At the scan-rate of 20 mV $s^{-1}$, the electrode can provide at 0 °C ∼85% of the capacitance at 20 °C. Plotting the capacitance versus $1/T$ gives an "apparent" activation energy of 10.3 kJ $mol^{-1}$, which is close to the activation energies for equivalent conductivities of alkali ions in aqueous solution [18]. It may suggest that the rate-limiting step to the capacitance in the present cell resides in ion diffusion in electrolyte solution. Furthermore, when cycled within the potential range of ±1.0 V, the cell exhibited no capacity decay after 3000 cycles (Fig. 10). As shown, this is in great contrast to a-$MnO_2$ electrode, which typically shows significant capacitance decay after only a few hundred cycles in the same electrolyte solution.

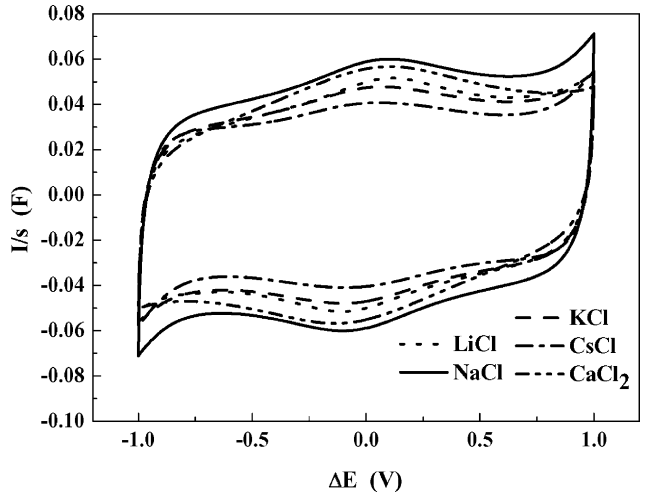


Fig. 7. Voltammograms for symmetric cell of $MnFe_2O_4$/CB in different 1 M aqueous electrolytes (scan-rate: 20 mV $s^{-1}$).

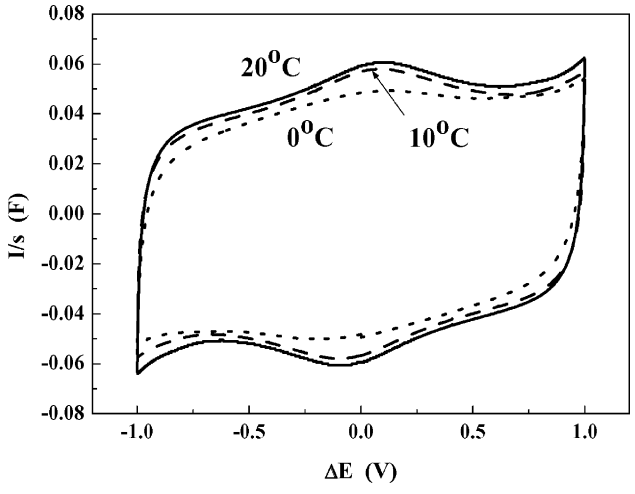


Fig. 9. Voltammograms of symmetric cell of $MnFe_2O_4$/CB with 1 M NaCl electrolyte under different operating temperatures (scan-rate: 20 mV $s^{-1}$).

Upon being charged under a constant current, the cell electrodes showed potential increase until reaching a plateau, where the applied current is equal to the leakage current (Fig. 11). With an operating potential of 1 V, the leakage current is ~10 mA $g^{-1}$, which corresponds to ~0.3 mA $F^{-1}$ of a symmetric cell.

The self-discharge behaviors of the composite electrodes were characterized by recording chrono-voltage curves on open-circuit after individual symmetric cell being charged to 1.0 V. Fig. 12 compares the curves for pure CB cell and the composite cells of difference CB-to-ferrite weight ratios. As shown, the CB cell exhibits the fastest voltage decay, and the decaying rate is progressively reduced with increasing ferrite content up to 70%. The decreasing trend in the decaying rate with ferrite content matches with the increasing trend in specific capacitance of the composite electrodes, which will be described in the following section. This can be understood by considering the relation: $dV/dt = (1/C)i_s$, where $C$ is capacitance and $i_s$, leakage current. Therefore, the voltage decaying rate decreases with increasing capacitance. It is also noted (Fig. 12) that the voltage decaying rate of the a-$MnO_2$ cell is similar to the composite cells with ferrite contents ≥50%.

### 3.3. Optimization of electrode composition

The presence of CB in the electrode does have several advantages. For one, it helps to disperse the ferrite particles so as to increase the surface area of the ferrite materials. Secondly, the pores of CB serve as reservoirs of the electrolyte. Finally, the CB component provides a high-conducting path within the electrode. However, its specific capacitance (~10.0 F $g^{-1}$ in 1 M NaCl at 20 mV $s^{-1}$) is much lower than that of the ferrite phase. Effort was hence made to optimize the ferrite:CB weight ratio for maximum capacitance. Fig. 13 shows the voltammograms of electrodes having different ferrite contents acquired in $NaCl_{(aq)}$ electrolyte. All the current profiles still show characteristics of a capacitor. The electrode capacitance first increases and then decreases with increasing ferrite content with the max-

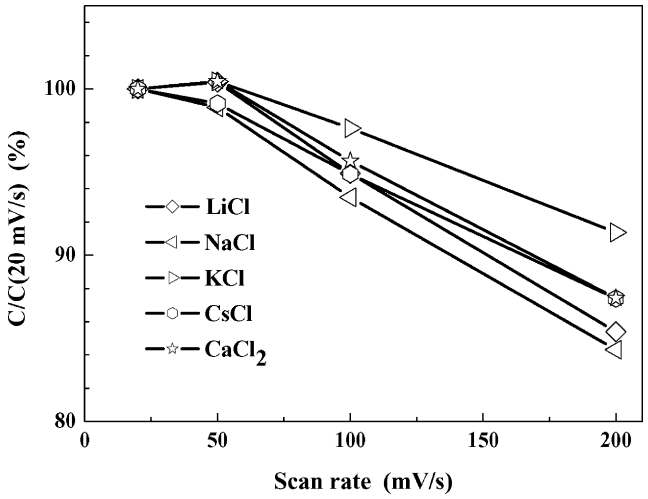


Fig. 8. Effect of scan-rate on capacitance of $MnFe_2O_4$/CB electrode in different electrolytes. $C$(20 mV $s^{-1}$) represents the capacitance determined at 20 mV $s^{-1}$.

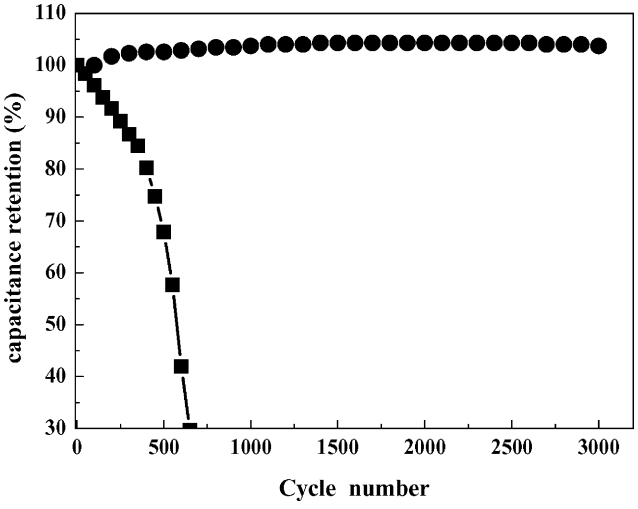


Fig. 10. Capacitance retention of symmetric cells of (●) $MnFe_2O_4$/CB and (■) a-$MnO_2$ in 1 M NaCl electrolyte at 20 °C with an operating potential range of 0.0–1.0 V.

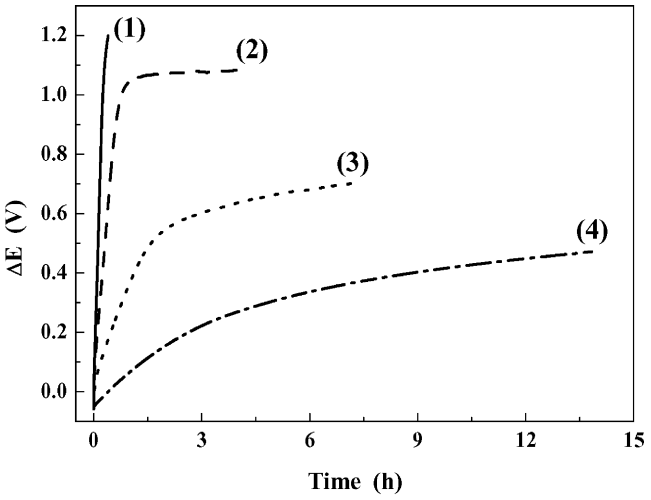


Fig. 11. Chronopotentiometric curves under constant current charging for symmetric cell of $MnFe_2O_4$/CB in 1 M NaCl electrolyte at 20 °C. Key: (1) 25 mA $g^{-1}$, (2) 10 mA $g^{-1}$, (3) 2.5 mA $g^{-1}$, and (4) 1 mA $g^{-1}$.

imum capacitance of ∼65 F $g^{-1}$ at ferrite:CB = 7:3 (Fig. 14a). Taking into account of the theoretical densities of carbon and the ferrite, ∼2.2 and 4.9 g $cm^{-3}$, respectively, and BET data gives the volume ratios of ferrite:CB:pore ∼1.0:1.0:0.9 for the optimum powder. The optimum weight ratio remains the same for the composite powders calcined over the entire temperature between 350 and 500 °C (Fig. 14a). One notes the dramatic drop in capacitance as the ferrite content passes over the optimum value. For the 70%-ferrite electrode calcined at 350 °C, its rate dependence follows closely to that shown in Fig. 8, and exhibited a capacitance of ∼55 F $g^{-1}$ at the scan-rate of 200 mV $s^{-1}$. This corresponds to a specific energy of 7.6 Wh $kg^{-1}$ at the power density of 11 kW $kg^{-1}$.

The capacitances of the ferrite phase in these composite electrodes are estimated by assuming the contribution of the CB substrate remains constant (∼10.0 F $g^{-1}$). As mentioned above (Fig. 3), the overall BET surface area is in fact reduced by loading of the ferrite material, particularly after calcination. Thus, the

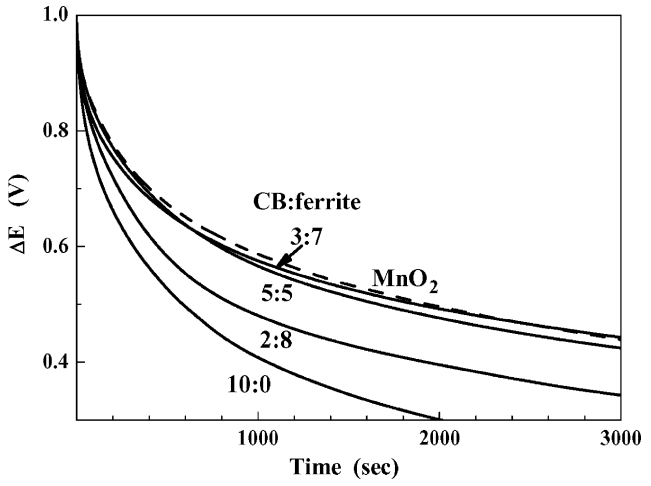


Fig. 12. Self-discharge for symmetric cells of CB, $MnFe_2O_4$/CB composites of different weight ratios, and a-$MnO_2$ (dashed) in 1 M NaCl solution at 20 °C.

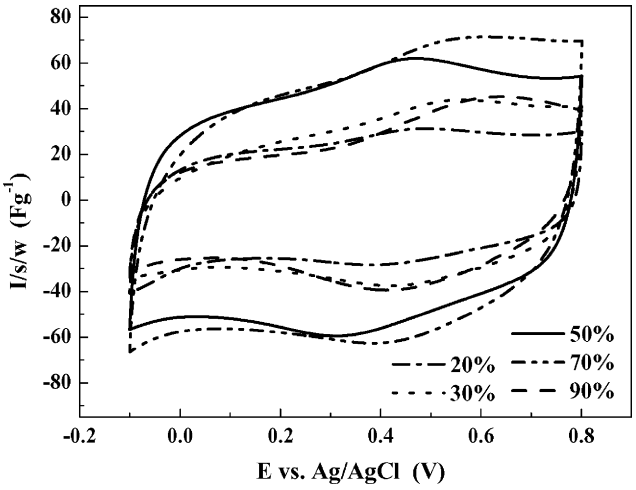


Fig. 13. Voltammograms of the composite electrodes of different ferrite contents in 1 M NaCl electrolyte at scan-rate of 20 mV $s^{-1}$.

assumption gives an upper bound to the contribution of the CB component, and hence a lower bound to the ferrite phase in every electrode. The estimated specific capacitances for the ferrite material in different electrodes are summarized in Fig. 14b. For

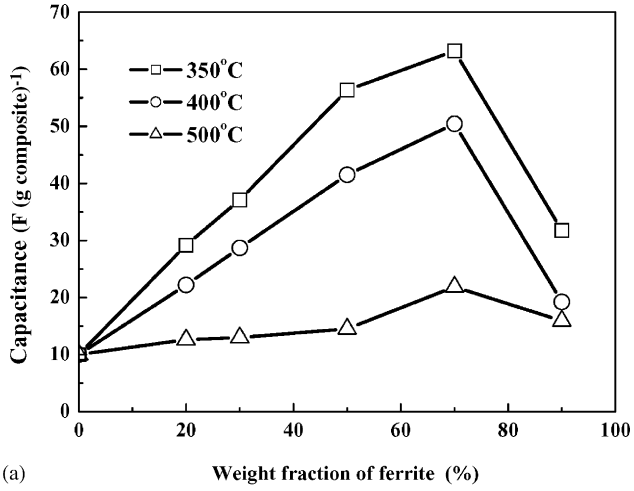


(a)

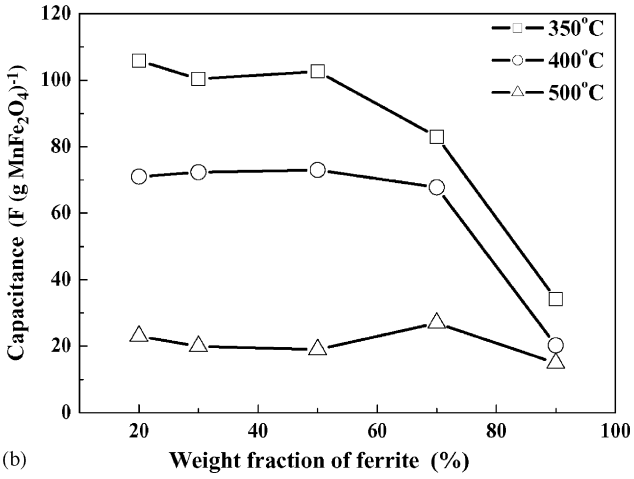


(b)

Fig. 14. The specific capacitances based on: (a) the total electrode weight and (b) the $MnFe_2O_4$ component as a function of ferrite contents.

those calcined at either 400 or 350 °C, the specific capacitance of the ferrite component remains fairly constant with weight ratio up to the loading of 50%, above which the specific capacitance starts to drop. It is believed that agglomeration among the ferrite particles becomes increasingly significant above this threshold loading. The saturation capacitance for the ferrite phase calcined at 350 °C is ∼105 F $g^{-1}$ (Fig. 14b). The data for 500 °C does not exhibit the same trend. This may be due to the fact that the capacitances of these electrodes are low, and the errors arising form the assumption of capacitance for CB are too large to neglect.

## 4. Conclusion

$MnFe_2O_4$–CB composite powders have been synthesized and characterized for their electrochemical properties. The composite shows pseudocapacitance in solutions of chloride, sulfate and sulfite salts of alkali and alkaline cations, with NaCl solution giving the highest capacitance. For the chlorides and sulfates electrolytes, the pseudocapacitance is associated with charge-transfer at both the Mn and Fe sites. In 1 M NaCl, the composite electrode exhibits an operating potential window of 1.0 V with a maximum leakage current of 0.3 mA $F^{-1}$, and it exhibits superior cycling stability to the a-$MnO_2$ electrode in the same electrolyte solution. The specific capacitance and self-discharge behavior of the composite depend strongly on the ferrite content, and the optimum capacitance occurs at ferrite:CB weight ratio of 7:3.

## Acknowledgement

This work is supported by National Science Council of Republic of China under contract number NSC 94-2214-E-002-003. The authors thank Dr. Jyh-Fu Lee and Mr. Din-Goa Liu at NSRRC for their assistance on XANES analysis.

## References

[1] B.E. Conway, J. Electrochem. Soc. 138 (1991) 1539–1548.
[2] B.E. Conway, V. Briss, J. Wojtowicz, J. Power Sources 66 (1997) 1–14.
[3] R. Kötz, M. Carlen, Electrochim. Acta 45 (2000) 2483–2498.
[4] S. Trasatti, G. Buzzanca, J. Electroanal. Chem. 29 (1971), App. 1–5.
[5] J.P. Zhang, P.J. Cygan, T.R. Jow, J. Electrochem. Soc. 142 (1995) 2699–2703.
[6] J.P. Zheng, Electrochem. Solid-State Lett. 2 (1999) 359–361.
[7] H.Y. Lee, J.B. Goodenough, J. Solid State Chem. 144 (1999) 220–223.
[8] H.Y. Lee, V. Manivannan, J.B. Goodenough, C. R. Acad. Sci. Paris t. 2 Série II c (1999) 565–577.
[9] R.N. Reddy, R.G. Reddy, J. Power Sources 124 (2003) 330–337.
[10] C.C. Hu, T.W. Tsou, Electrochem. Commun. 4 (2002) 105–109.
[11] S.-C. Pang, M.A. Anderson, T.W. Chapman, J. Electrochem. Soc. 147 (2000) 444–450.
[12] N.L. Wu, Y.P. Lan, C.Y. Han, S.Y. Wang, L.R. Shiue, Proceedings of the 201st Meeting of American Electrochemical Society, Philadelphia, PA, USA, May 12–17, 2002.
[13] N.L. Wu, S.Y. Wang, C.Y. Han, D.S. Wu, L.R. Shiue, J. Power Sources 113 (2003) 173–178.
[14] S.Y. Wang, N.L. Wu, J. Appl. Electrochem. 33 (2003) 345–348.
[15] S.Y. Wang, K.C. Ho, S.L. Kuo, N.L. Wu, J. Electrochem. Soc. 153 (2006) A75–A80.
[16] S.L. Kuo, N.L. Wu, Electrochem. Solid-State Lett. 8 (2005) A495–A499.
[17] M.A. Denecke, W. Gunsser, G. Buxbaum, P. Kuske, Mater. Res. Bull. 27 (1992) 507–514.
[18] T. Bastug, S. Kuyucak, Chem. Phys. Lett. 408 (2005) 84–88.